Journal of Power Sources 192 (2009) 78–83

Contents lists available at ScienceDirect

Journal of Power Sources

journal homepage: www.elsevier.com/locate/jpowsour

# Structure, thermal stability and electrical properties of $Ca(V_{0.5}Mo_{0.5})O_3$ as solid oxide fuel cell anode

A. Aguadero[a,*], C. de la Calle[b], J.A. Alonso[b], D. Pérez-Coll[a], M.J. Escudero[a], L. Daza[a,c]

[a] CIEMAT, Av. Complutense 22, 28040 Madrid, Spain
[b] Instituto de Ciencia de Materiales de Madrid (CSIC), Cantoblanco, 28049 Madrid, Spain
[c] Instituto de Catálisis y Petroleoquímica (CSIC), C/Marie Curie 2, Campus Cantoblanco, 28049 Madrid, Spain

ARTICLE INFO

*Article history:*
Received 15 October 2008
Received in revised form
26 November 2008
Accepted 10 December 2008
Available online 24 December 2008

*Keywords:*
Electrode
Solid oxide fuel cells
Perovskite
Ca–V–Mo

ABSTRACT

The $Ca(V_{0.5}Mo_{0.5})O_3$ perovskite has been prepared in order to study its potential use as anode in SOFC. The crystal structure has been refined, by neutron powder diffraction, in the orthorhombic *Pbnm* space group (no. 62). The electrical conductivity values were over 525 S cm$^{-1}$ in the studied temperature range (25–800 °C). The sample is stable under reducing working conditions ($H_2/N_2$ 10:90, 25–900 °C). This orthorhombic phase transforms at 500 °C in air to the tetragonal $I4_1/a$ scheelite phase. This transition is reversible and, due to the fact that the thermal expansion coefficients of both, the reduced and oxidized phases, are very similar and match well with those of the other cell components ($(10–13) \times 10^{-6}$ K$^{-1}$) this materials are presented as excellent candidates as anodes in SOFCs.



## 1. Introduction

Materials with perovskite-like structure are receiving great attention due to their vast range of possible applications. This is mainly due to their capability to present both, electronic and ionic conductivity. Among the huge variety of compounds with the perovskite-like structure, $CaVO_3$ and $CaMoO_3$ have been observed to present Pauli paramagnetic and metallic behaviour with one of the highest conductivity values reported at room temperature ($\sim 10^4$ S cm$^{-1}$) [1]. Moreover, oxides with transition metals from the V or VI groups have been observed to present high catalytic activity for some oxidation reactions. For instance, vanadium containing oxides are being studied for selective oxidation of hydrocarbon molecules [2–4] and Mo–V–O oxides are being investigated for some oxidation reactions due to their lower reducibility and oxidative dehydrogenation rates [5–7]. On the other hand, oxides consisting on combination of two transition metals have been used to enhance the structural stability in different atmospheres [8].

Nowadays, the development of an adequate anode material for solid oxide fuel cells (SOFCs) is of great interest. One of the targets is to obtain a mixed electronic-ionic conductor stable in the anodic atmosphere and with high catalytic activity for fuel oxidation. In this way, $Ca(V_{0.5}Mo_{0.5})O_3$ is presented as a promising candidate as anode material.

The crystal structure of $Ca(V_{0.5}Mo_{0.5})O_3$ has been previously defined from synchrotron X-ray powder diffraction (SXPD) data in the orthorhombic *Pnma* space group (no. 62) with no signs of long-range ordering of V and Mo atoms into a supercell; it has been described to be highly conductive and Pauli paramagnetic at low temperatures (10–300 K) [9].

The aim of this work is to study the stability region of the $Ca(V_{0.5}Mo_{0.5})O_3$ phase, to give accurate structural details from neutron powder diffraction (NPD) data and to investigate its thermal expansion and electrical behaviour under reducing atmosphere, in order to evaluate its potential use as anode material in SOFCs.

## 2. Experimental

The synthesis of $Ca(V_{0.5}Mo_{0.5})O_3$ was performed by the citrate route. Stoichiometric amounts of analytical grade of the following reactants: $CaCO_3$, $NH_4VO_3$ and $(NH_4)_6Mo_7O_{24}{\cdot}4H_2O$ were dissolved in citric acid (10%). The formed solution was dehydrated leading to an organic resin which was dried at 120 °C and slowly decomposed at 600 °C for 12 h. The reactive precursor powder was calcined first at 900 °C, in 5% forming gas, and after at 1200 °C in 1% of $H_2$/Ar.

The initial structural characterization of the obtained products was performed by X-ray diffraction in a Bruker-ax D8 equipment (40 kV, 30 mA) in Bragg–Brentano reflection geometry with Cu Kα

* Corresponding author. Tel.: +34 91 3349000; fax: +34 91 3720623.
*E-mail address:* ainara.aguadero@gmail.com (A. Aguadero).

0378-7753/$ – see front matter © 2008 Elsevier B.V. All rights reserved.
doi:10.1016/j.jpowsour.2008.12.035

radiation ($\lambda$ = 1.5418 Å) for phase identification and to asses phase purity.

X-ray-thermo-diffractometry study was performed with an Anton Parr HTK 1200N temperature vessel, provided with a window of Kapton. The sample was placed in an alumina sample holder which was introduced into the furnace of the diffractometer. It was heated in still air from room temperature to 1000 °C at a controlled rate of 10 °C min$^{-1}$, and cooled again to room temperature.

Neutron powder diffraction data were collected with the HRPT diffractometer from the SINQ spallation source at the Paul Scherrer Institute, Zurich. The patterns were collected at room temperature with a wavelength of 1.494 Å. The sample was placed on a 6 mm of diameter vanadium can and the measurements were performed in the high intensity mode with 2 h of collection time. The refinement of the crystal structure was performed by the Rietveld method, using the WinPLOTR [10,11] application from the FULLPROF refinement program [12]. A pseudo-Voigt function was chosen to generate the line shape of the diffraction peaks. The coherent scattering lengths for Ca, V, Mo and O were: 4.70, −0.0382, 6.715 and 5.803 fm, respectively. The following parameters were refined in the final run: scale factor, background coefficients, zero-point error, pseudo-Voigt corrected for asymmetry parameters, positional coordinates and isotropic thermal factors.

Thermogravimetric (TG) and differential thermal analysis (DTA) curves in air were obtained using a Stanton STA 781 instrument in the range of 25–900 °C whereas in reducing conditions they were recorded in a Mettler Toledo STAR SW 9.01 instrument, in the 30–900 °C temperature range, under a 10% $H_2$ forming gas flow (100 ml min$^{-1}$).

Dense compounds were required in order to evaluate the thermal expansion and electrical conductivity. For this purpose the powder was uniaxially pressed (∼1 Tm) into a rectangular bar for thermal expansion analysis and into cylindrical pellet for electrical characterization. The samples were calcined at 1180 °C for 4 h in an atmosphere of 1% $H_2$/Ar. The thermal expansion was determined by dilatometric analysis using a Linseis L75/1550C dilatometer in air and 10% $H_2$ atmospheres. The electrical conductivity was evaluated by two different methods as a function of the atmosphere. The dc Van der Pauw four-probe method was used for measuring the reduced sample in 10% $H_2$ forming gas between 25 and 800 °C. A current load of 1 A was applied by a dc dual output power supply (E3646 A Agilent Technologies) and the potential drop recorded by a Fluke 179 True RMS Multimeter. Moreover, the electrical conductivity was measured as a function of the oxygen partial pressure in the $pO_2$ range of $10^{-20}$ to $10^{-14}$ atm. For this purpose, the temperature and oxygen partial pressure were stabilized at 750 °C in a mixture of 10% $H_2$/90% $N_2$; then the $H_2$ flow was closed and the system was slowly oxidized under $N_2$ flow. A YSZ oxygen sensor was used to obtain the oxygen partial pressure of the system and the electrical conductivity was measured as previously described.

On the other hand, due to the low electronic conductivity of the oxidized sample, an ac impedance analysis was required in order to determine the electrical conductivity in air. For this purpose, a Metalor 6082 Pt ink was symmetrically painted as a current collector on both surfaces of the pellet. Impedance spectroscopy was performed with an AUTOLAB PGSTAT 302, ECO CHEMIE equipment, in the range of $10^{-2}$ to $10^{6}$ Hz, with an excitation voltage of 50 mV, and decreasing the temperature from 900 to 500 °C.

## 3. Results and discussion

### 3.1. Thermal analysis stability

In order to analyze the stability of $Ca(V_{0.5}Mo_{0.5})O_3$ to the usual oxidation–reduction cycles that must abide an anode electrode in a SOFC device, TG and DTA measurements were performed in both, air and 10% of $H_2$ forming gas atmospheres between 25 and 1000 °C. The DTA curve shows the presence of two peaks at 555 and 1003 °C (Fig. 1a) when heating the sample in air. The first one is an exothermic and irreversible process and could be attributed to the oxygenation of the sample as it is indicated by the TG curve (Fig. 1b). The second one reveals an endothermic and reversible process.

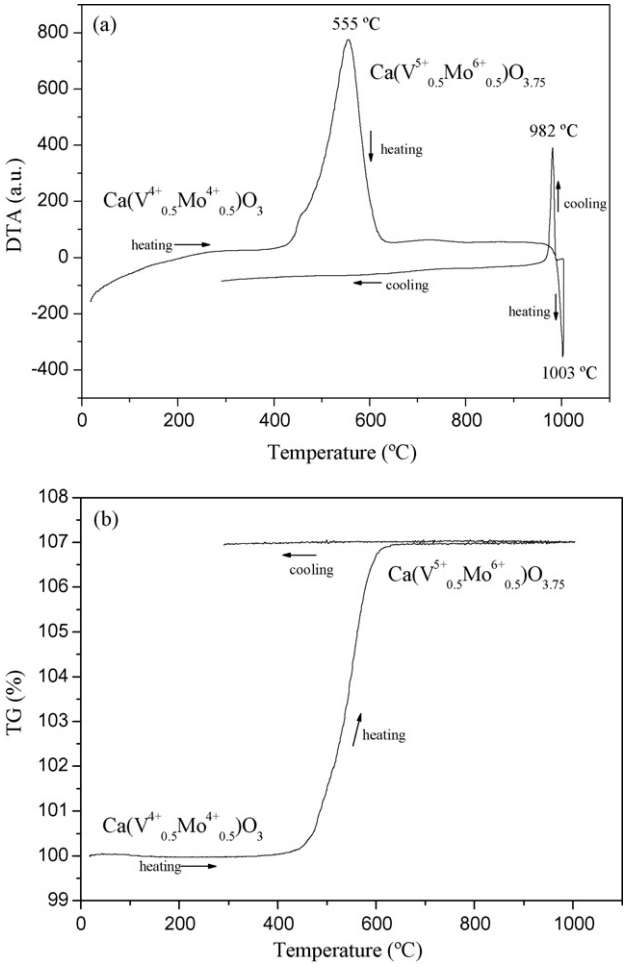


**Fig. 1.** Thermal analysis of the perovskite $Ca(V_{0.5}Mo_{0.5})O_3$ in air between 25 and 1000 °C: (a) DTA curve and (b) TG curve.

The TG/DTA measurement in 10% $H_2$ forming gas does not reveal either the weight loss or gain or the presence of any structural transition.

In order to appropriately investigate the observed processes a meticulous structural study was performed.

### 3.2. Structural characterization

The crystal structure refinement of the $Ca(V_{0.5}Mo_{0.5})O_3$ phase, obtained in reducing atmosphere, was performed from NPD data collected at room temperature. The structure was defined in the orthorhombic *Pbnm* (no. 62) space group, with lattice parameters $a$ = 5.4030(1) Å, $b$ = 5.4642(2) Å, $c$ = 7.6812(2) Å and $V$ = 226.77(1) Å$^3$ in agreement with data of Karen et al. [9] obtained by synchrotron X-ray powder diffraction. The atoms were placed in the special positions of the space group given in Table 1. V and Mo are distributed at random at 4b positions; our NPD data do not show any evidence of long-range ordering of V and Mo, which would have resulted in

**Table 1**
Unit-cell, positional and thermal parameters for $Ca(V_{0.5}Mo_{0.5})O_3$ perovskite in the orthorhombic *Pbnm* space group from NPD data at RT.

| | |
|---|---|
| *a* (Å) | 5.4030(1) |
| *b* (Å) | 5.4642(2) |
| *c* (Å) | 7.6812(2) |
| *V* (Å)$^3$ | 226.770(7) |
| Ca 4*c* (*x*, *y*, 1/4) | |
| *x* | 0.9951(5) |
| *y* | 0.0365(3) |
| *B* (Å)$^2$ | 0.94(3) |
| V 4*b* (1/2, 0, 0) | |
| *B* (Å)$^2$ | 0.35(3) |
| Mo 4*b* (1/2, 0, 0) | |
| *B* (Å)$^2$ | 0.35(3) |
| O1 4*c* (*x*, *y*, 1/4) | |
| *x* | 0.0678(3) |
| *y* | 0.4842(3) |
| *B* (Å)$^2$ | 0.62(2) |
| O2 8*d* (*x*, *y*, *z*) | |
| *x* | 0.7085(2) |
| *y* | 0.2905(2) |
| *z* | 0.0354(1) |
| *B* (Å)$^2$ | 0.62(2) |
| Reliability factors | |
| $\chi^2$ | 1.87 |
| $R_p$% | 2.78 |
| $R_{wp}$% | 3.53 |
| $R_{Bragg}$% | 2.95 |

an additional lowering of the symmetry in a superstructure of the perovskite. In order to accommodate the divalent calcium in the A sub-cell of the perovskite the structure of $Ca(V_{0.5}Mo_{0.5})O_3$ undergoes a slight octahedral tilting distortion (Table 2), which lowers the symmetry from the undistorted cubic perovskite (space group P*m*-3*m*) to the orthorhombic *Pbnm* space group as it has been also observed for the $CaVO_3$ [1] and the $CaMoO_3$ [13]. The goodness of the Rielveld fit is shown in Fig. 2.

**Table 2**
Main bond distances (Å) and selected angles (°) for orthorhombic $Ca(V_{0.5}Mo_{0.5})O_3$ determined from NPD data at RT.

| | |
|---|---|
| $CaO_{10}$ polyhedra | |
| Ca–O1 | 2.478(3) |
| Ca–O1[a] | 3.043(2) |
| Ca–O1[a] | 3.054(3) |
| Ca–O1 | 2.379(4) |
| Ca–O2 (×2) | 2.653(2) |
| Ca–O2 (×2) | 2.394(2) |
| Ca–O2 (×2) | 2.651(2) |
| <Ca–O>$_8$ short | 2.532 |
| $BO_6$ octahedra (B = Mo,V) | |
| B–O1 (×2) | 1.9567(4) |
| B–O2 (×2) | 1.965(1) |
| B–O2 (×2) | 1.966(1) |
| <B–O> | 1.963 |
| Angles around B (B = Mo,V) | |
| O1–B–O1 | 180.00(3) |
| O1–B–O2 | 90.39(8) |
| O1–B–O$_2$ | 89.34(8) |
| O1–B–O2 | 90.66(7) |
| O1–B–O2 | 89.61(7) |
| O2–B–O2 | 89.54(8) |
| O2–B–O2 | 90.46(8) |
| O2–B–O2 | 180.00(1) |
| B–O1–B | 157.85(1) |
| B–O2–B (×2) | 155.59(9) |
| <B–O–B> | 156.34 |

[a] Long Ca–O distance.

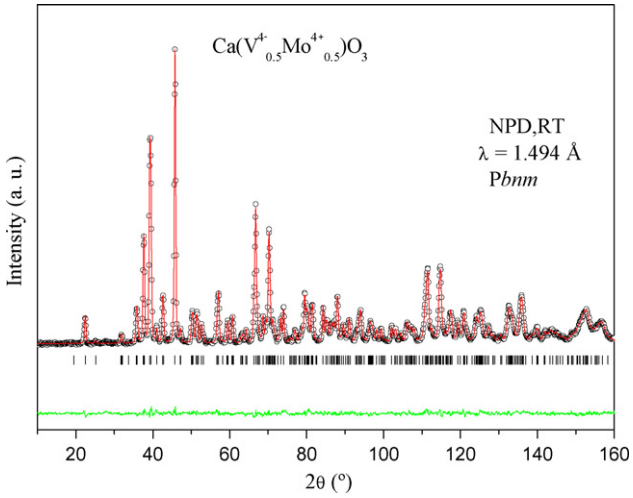


**Fig. 2.** Rietveld plot refined from NPD data of the perovskite $Ca(V_{0.5}Mo_{0.5})O_3$ phase.

The tilting of the $(V,Mo)O_6$ octahedra can be estimated as $\phi = (180 - \langle B–O–B \rangle)/2 = 11.83°$. As shown in Table 2, Ca–O distances in the rather distorted $CaO_{12}$ polyhedron range from 2.394 to 3.054 Å; the effective coordination of $Ca^{2+}$ cations can be considered as eightfold, only considering the bond-lengths below 2.65 Å, with an average <Ca–O>$_8$ short value of 2.532 Å which compares well with that expected from the ionic radii sums [14] of 2.52 Å for $^{VIII}Ca^{2+}$ (i.r.: 1.12 Å). For the (Mo,V)–O bonds the average distance of 1.963 Å is somewhat shorter than expected, of 1.98 Å for $^{VI}V^{4+}$ ions (i.r.: 0.58 Å) and 2.05 Å for $^{VI}Mo^{4+}$ ions (i.r.: 0.65 Å).

### 3.3. Thermodiffractometry in air atmosphere

Thermo-X-ray diffraction studies were performed in still air from room temperature (RT) up to 1000 °C. Two-phase transitions have been detected and characterized in agreement with the information obtained from the DTA measurements in air (Fig. 1a). The first one at 555 °C is a reconstructive phase transition, non-reversible in air, that corresponds to the transformation of the perovskite-like structure $Ca(V_{0.5}Mo_{0.5})O_3$ to the oxidized tetragonal $Ca(V_{0.5}Mo_{0.5})O_{3.7}$ scheelite like structure followed by the segregation of the $Ca_2V_2O_7$ pyrochlore phase that is thermodynamically very stable at high temperatures and compete with the formation of the scheelite phase (Fig. 3). The second transformation at 1000 °C, is a reversible endothermic, first order reconstructive transition (Fig. 1) which corresponds to the fusion process of the segregated calcium pyrochlore. Fig. 4 shows the XRD diagram collected at 1000 °C in which the characteristic reflections of the schellite phase can only be observed, since the pyrochlore phase is in an amorphous state.

On the other hand, the Rietveld refinement from the X-ray diffraction data obtained *in situ* at 1000 °C for the oxidized sample $Ca(V_{0.5}Mo_{0.5})O_{3.75}$ reveals that this compound presents a tetragonal scheelite structure defined in the $I4_1/a$ space group (no. 88), with lattice parameters $a = 5.2922(8)$ Å, $c = 11.680(1)$ Å and $V = 327.2(1)$ Å. Ca atoms were located at 8*d* (0, 1/4, 5/8) positions; V and Mo atoms were distributed at random at the 8*c* (0, 1/4, 1/8) positions and oxygen atoms at 16*f* (*x*, *y*, *z*) positions. Refinements of 18 profile and atomic parameters resulted in final residuals of $R_{Bragg} = 7.7\%$ and $\chi^2 = 1.6$. The refinement of the occupancy factor for the oxygen sublattice led to an oxygen stoichiometry of 3.7(1), in agreement with the nominal formula. A good fit between the observed and calculated profiles was obtained; the Rietveld fit for $Ca(V_{0.5}Mo_{0.5})O_{3.75}$

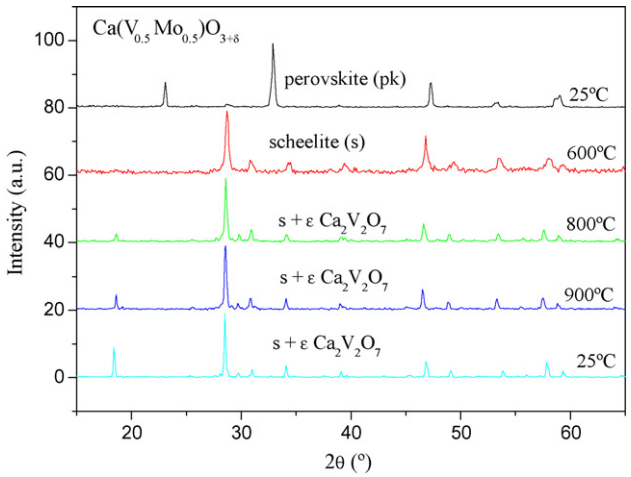


**Fig. 3.** Thermo-X-ray diffraction diagram performed in still air from 2 5 °C up to 900 °C and cooled down again to 25 °C.

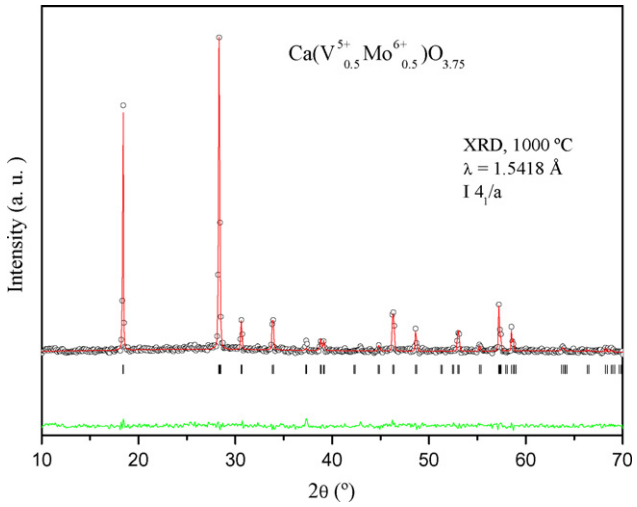


**Fig. 5.** Rietveld plot refined from XRD data at 1000 °C of the scheelite $Ca(V_{0.5}Mo_{0.5})O_{3.7}$ phase.

from XRD data is shown in Fig. 5. The heat treatment of the oxidized sample at 1000 °C in 10% $H_2$ forming gas lead back to the stabilization of the reduced perovskite phase.

### 3.4. Thermal treatments in reducing conditions

Fig. 6 shows the XRD patterns at RT of the $Ca(V_{0.5}Mo_{0.5})O_3$ perovskite as prepared (a) or after a thermal treatment at 900 °C in 10% $H_2$ forming gas atmosphere (b). The results evidence the absence of structural instability of the perovskite phase when heating the sample in reducing conditions.

### 3.5. Thermal expansion

In order to evaluate the possible application of the $Ca(V_{0.5}Mo_{0.5})O_3$ perovskite as anode in SOFC, the thermal expansion of both, the oxidized (scheelite) and the reduced (perovskite) phases have been evaluated on sintered pellets. Fig. 7 shows the linear thermal expansion of $Ca(V_{0.5}Mo_{0.5})O_3$ in 10% $H_2$ forming gas and of $Ca(V_{0.5}Mo_{0.5})O_{3.75}$ in air between 100 and 900 °C. The cell volume of the perovskite and the scheelite phases were 226.770(7) and 327.1 $Å^3$, respectively which indicates a variation of about 30% of volume. However, the thermal expansion coefficients obtained from the slope of the lines are very close to each other, with values of 10 and $13 \times 10^{-6}\,K^{-1}$ for the oxidized and reduced sample, respectively, which are in the range of typical values expected for SOFC components. These low differences would avoid problems of cracking during oxidation–reduction cycles.

### 3.6. Electrical conductivity

The electrical conductivity of the reduced $Ca(V_{0.5}Mo_{0.5})O_3$ perovskite was measured on a dense pellet in 10% $H_2$ forming gas atmosphere by the Van der Pauw four-probe method between 25 and 800 °C. Fig. 8 evidences a metallic-like behaviour for all the temperature range under study. In the usual temperature conditions of a SOFC anode (650–800 °C) the sample displays conductivity values between 525 S $cm^{-1}$ ($T$ = 800 °C) and 632 S $cm^{-1}$ ($T$ = 650 °C), which fulfil the specified requirements for anode materials in SOFCs.

The electrical conductivity of the oxidized $Ca(V_{0.5}Mo_{0.5})O_{3.75}$ scheelite was measured on a dense pellet in air by ac impedance spectroscopy between 25 and 900 °C. In this phase the V(V) and Mo(VI) cations are in their maximum oxidation state and, there-

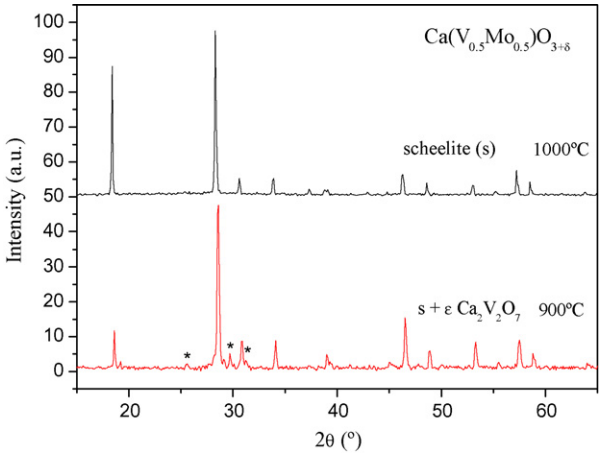


**Fig. 4.** XRD diagrams after thermal treatments at 900 and 1000 °C in air, showing the fusion of the pyrochlore $Ca_2V_2O_7$ phase at 1000 °C, which transforms into an amorphous phase. The asterisk (*) indicates the diffraction peaks of the $Ca_2V_2O_7$ phase.

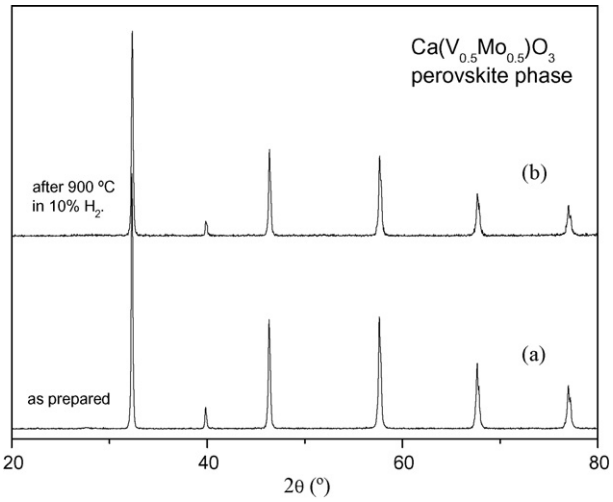


**Fig. 6.** XRD diagram of $Ca(V_{0.5}Mo_{0.5})O_3$: (a) before and (b) after the thermogravimetric study between 25 and 900 °C in 10% of $H_2$ forming gas.

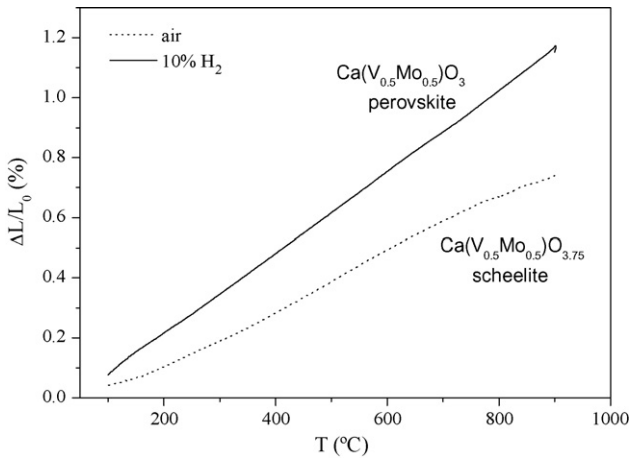


**Fig. 7.** Thermal expansion of the scheelite and the perovskite phases in air and 10% $H_2$ forming gas, respectively.

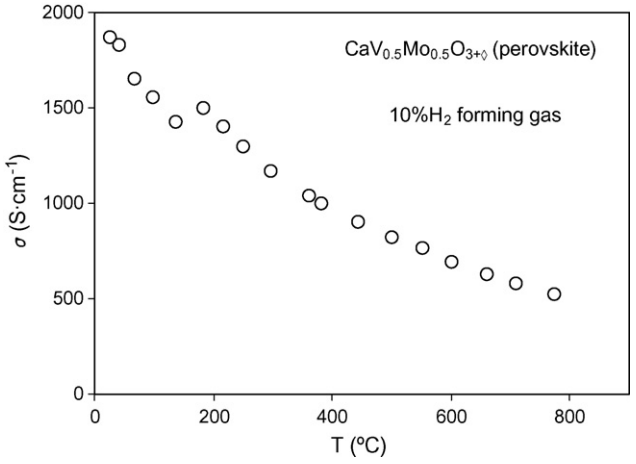


**Fig. 8.** Electrical conductivity of the perovskite $Ca(V_{0.5}Mo_{0.5})O_3$ phase in 10% $H_2$ forming gas between 25 and 800 °C.

fore, no electronic conduction is expected. However, the electrical conductivity observed is in the range $10^{-4}$ to $10^{-5}$ S cm$^{-1}$ between 700 and 900 °C. This residual conductivity could be attributed to an ionic conductivity due to the motion of the oxygen vacancies

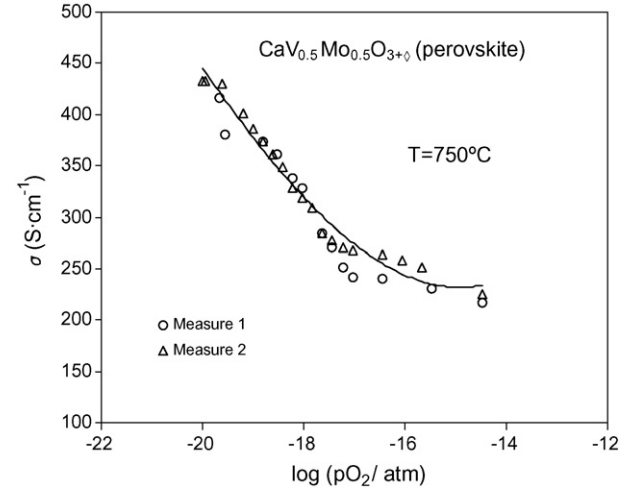


**Fig. 9.** Dependence of conductivity on oxygen partial pressure at 750 °C for the perovskite $Ca(V_{0.5}Mo_{0.5})O_3$.

driven by the partial substitution of Mo(VI) by V(V) that generates an oxygen hypo-stoichiometry of 3.75 with regard to that expected for the stoichiometric scheelite, $ABO_4$. In fact, the refinement of the oxygen occupancy of the scheelite phase confirmed the presence of oxygen vacancies, which are in the origin of the observed electrical conductivity in air.

It was observed that the perovskite material displays high values of electronic conductivity under reducing conditions. However, when this phase is oxidized to the scheelite structure becomes it an insulator. In order to evaluate the variation of the electrical conductivity of the $Ca(V_{0.5}Mo_{0.5})O_3$—perovskite with the oxygen partial pressure the electrical conductivity was measured in the $10^{-20}$ to $10^{-14}$ $pO_2$ range. Fig. 9 shows a slight decrease of the electrical conductivity with the increase of the oxygen partial pressure that could be attributed to the partial oxidation of V(IV) and Mo(IV) leading to a decrease in the charge carriers density. This slight variation was evaluated with a slope of about −1/10 in the log(conductivity) versus log($pO_2$) representation. However, the electrical conductivity is higher than 220 S cm$^{-1}$ in all the studied oxygen partial pressure range.

## 4. Conclusions

In the present work the perovskite $Ca(V_{0.5}Mo_{0.5})O_3$ has been evaluated as possible anode in SOFC. The crystal structure has been refined by NPD in the orthorhombic *Pbnm* space group. Under reducing conditions (10% $H_2$ forming gas), the electrical conductivity presents values well above 525 S cm$^{-1}$ in all the temperature range under study (25–800 °C). Moreover, it was observed that the conductivity is only slightly decreased when the oxygen partial pressure increases with values above 220 S cm$^{-1}$ at 750 °C in the $pO_2$ range of $10^{-20}$ to $10^{-14}$ atm of $pO_2$ as required for anode materials in SOFCs, and the thermal expansion coefficient is around $13 \times 10^{-6}$ K$^{-1}$. The sample displays a great stability under reducing conditions, whereas it undergoes a phase transition to the oxidized scheelite $Ca(V_{0.5}Mo_{0.5})O_{3.75}$ phase while heating above 400 °C in air. This oxygenated phase presents a tetragonal $I4_1/a$ space group with conductivity values of $10^{-4}$ to $10^{-5}$ S cm$^{-1}$ in the 700–900 °C temperature range and an expansion coefficient of $10 \times 10^{-6}$ K$^{-1}$. This phase transition is totally reversible and it is expected not to lead to cracking problems during the cell operation as the expansion coefficients of the reduced and the oxygenated samples are very close to each other, and similar to the rest of the usual components of a SOFC. In summary, we can conclude that the $Ca(V_{0.5}Mo_{0.5})O_3$ is a promising material to be used as a SOFC anode.

## Acknowledgements

We thank the financial support of the Madrid Community with the project ENERCAM S-0505/ENE-304) and to the Spanish Ministry of Science and Innovation to the project MAT2007-60536. We are grateful to PSI for making all the facilities available. One of the authors (D.P.-C.) also wishes to thank to the Science and Innovation Ministry for financial support by "Juan de la Cierva Program".

## References

[1] B.L. Chamberland, P.S. Danielson, J. Solid State Chem. 3 (1971) 243–247.
[2] R.K. Grasselli, Catal. Today 49 (1999) 141–153.
[3] T. Blasco, J.M. López-Nieto, Appl. Catal. A 157 (1997) 117–142.
[4] E.A. Mamedow, V. Cortés Corberán, Appl. Catal. A 127 (1995) 1–40.
[5] A. Bielanski, M. Najbar, Appl. Catal. A 157 (1997) 223–261.
[6] M.A. Bañares, S.J. Khatib, Catal. Today 96 (2004) 251–257.
[7] S. Yang, E. Iglesia, A.T. Bell, J. Phys. Chem. B 109 (2005) 8987–9000.

[8] Y.H. Huang, R.I. Dass, Z.L. Xing, J.B. Goodenough, Science 312 (2006) 254–257.
[9] P. Karen, A.R. Moodenbaugh, J. Goldberger, P.N. Santhosh, P.M. Woodward, J. Solid State Chem. 179 (2006) 2120–2125.
[10] T. Roisnel, J. Rodriguez-Carvajal, in: R. Delhez, E.J. Mittenmeijer (Eds.), Proceedings of the Seventh European Powder Diffraction Conference (EPDIC 7), 2000, pp. 118–123.
[11] J. Rodriguez-Carvajal, T. Roisnel, International Union for Crystallography, Newletter N20 (May–August) Summer, 1998.
[12] J. Rodriguez-Carvajal, Physica B 192 (1993) 55–69.
[13] C. de la Calle, J.A. Alonso, M. García-Fernández, V. Pomjakushin, J. Solid State Chem. 179 (2006) 1636–1641.
[14] R.D. Shannon, Acta Crystallogr. A32 (1976) 751–767.